Virology 379 (2008) 181–190

Contents lists available at ScienceDirect

Virology

journal homepage: www.elsevier.com/locate/yviro

Membrane binding properties of EBV gp110 C-terminal domain; evidences for structural transition in the membrane environment

Sung Jean Park [a], Min-Duk Seo [a], Suk Kyeong Lee [b], Bong Jin Lee [a,*]

[a] National Research Laboratory, Research Institute of Pharmaceutical Sciences, College of Pharmacy, Seoul National University, San 56-1, Shillim-Dong, Kwanak-Gu, Seoul 151-742, Republic of Korea

[b] Research Institute of Immunobiology, Catholic Research Institutes of Medical Science, The Catholic University of Korea, 505 Banpo-dong, Seocho-Gu, Seoul 137-701, Republic of Korea

ARTICLE INFO

Article history:
Received 8 October 2007
Returned to author for revision 10 April 2008
Accepted 22 June 2008
Available online 8 August 2008

Keywords:
EBV
gp110
gB
Membrane
Circular dichroism
Micelle
NMR

ABSTRACT

Gp110 of Epstein–Barr virus (EBV) mainly localizes on nuclear/ER membranes and plays a role in the assembly of EBV nucleocapsid. The C-terminal tail domain (gp110 CTD) is essential for the function of gp110 and the nuclear/ER membranes localization of gp110 is ruled by its C-terminal unique nuclear localization signal (NLS), consecutive four arginines. In the present study, the structural properties of gp110 CTD in membrane mimics were investigated using CD, size-exclusion chromatography, and NMR, to elucidate the effect of membrane environment on the structural transition and to compare the structural feature of the protein in the solution state with that of the membrane-bound form. CD and NMR analysis showed that gp110 CTD in a buffer solution appears to adopt a stable folding intermediate which lacks compactness, and a highly helical structure is formed only in membrane environments. The helical content of gp110 CTD was significantly affected by the negative charge as well as the size of membrane mimics. Based on the elution profiles of the size-exclusion chromatography, we found that gp110 CTD intrinsically forms a trimer, revealing that a trimerization region may exist in the C-terminal domain of gp110 like the ectodomain of gp110. The mutation of NLS (RRRR) to RTTR does not affect the overall structure of gp110 CTD in membrane mimics, while the helical propensity in a buffer solution was slightly different between the wild-type and the mutant proteins. This result suggests that not only the helicity induced in membrane environment but also the local structure around NLS may be related to trafficking to the nuclear membrane. More detailed structural difference between the wild-type and the mutant in membrane environment was examined using synthetic two peptides including the wild-type NLS and the mutant NLS.

Introduction

Glycoprotein 110 (gp110) is essential for virus assembly *in vivo* (Lee and Longnecker, 1997; Lee et al., 1997) and localizes predominantly on the inner and outer membranes of the nucleus in infected cells. Gp110 is a large glycoprotein composed of 857 amino acids. It consists of a long stretch of the N-terminal domain, three potential membrane-spanning regions, and a C-terminal tail domain (Fig. 1). Interestingly, the C-terminal tail domain of gp110 (gp110 CTD, hereafter) locating in nucleoplasm provides signals that are responsible for the assembly of EBV nucleocapsids and their egression through the nuclear membrane (Lee and Longnecker, 1997). Some reports indicated that the residues 816 to 841 in the tail domain containing four consecutive arginines (RRRR) are essential for the retention in the nuclear/endoplasmic reticulum (ER) membranes (Lee and Longnecker, 1997; Lee, 1999). In addition, a mutagenesis experiment supported that not only the positive charge of consecutive arginines but also their proper structural configuration is an important factor for the localization of gp110 to the nuclear/ER membranes (Lee, 1999). More recently, it is revealed that its biological role is not limited to virus assembly: gp110 appears to be the critical component for EBV glycoprotein-mediated cell fusion (McShane and Longnecker, 2004) and the residues 802 to 816 in the C-terminal domain are necessary for the productive membrane fusion, while the residues 817 to 841 negatively regulate membrane fusion (Haan et al., 2001). While the biological importance of gp110 in the virus fusion and assembly were emphasized on, little is known about the structural characteristic of gp110. The recombinant gp110 CTD may be partially folded in a buffer condition but adopts more ordered structure in micelle solutions (Park et al., 2002). It is well known that some soluble proteins have the native molten-globule structures that facilitate binding to lipid bilayer (Song and Kim, 1997, Song et al., 2001; Lohner and Esser,1991) and that the molten-globule like conformation has a key role for membrane binding of proteins. In the present study, we investigated the membrane binding properties of gp110 CTD and the structural transition on membrane mimics by characterizing the fold of gp110 CTD in a buffer and membrane-mimicking conditions. In addition, to elucidate whether the disturbed ER/membrane localization by mutation of the nuclear

* Corresponding author. Fax: +82 2 872 3632.
E-mail address: lbj@nmr.snu.ac.kr (B.J. Lee).

0042-6822/$ – see front matter © 2008 Elsevier Inc. All rights reserved.
doi:10.1016/j.virol.2008.06.031

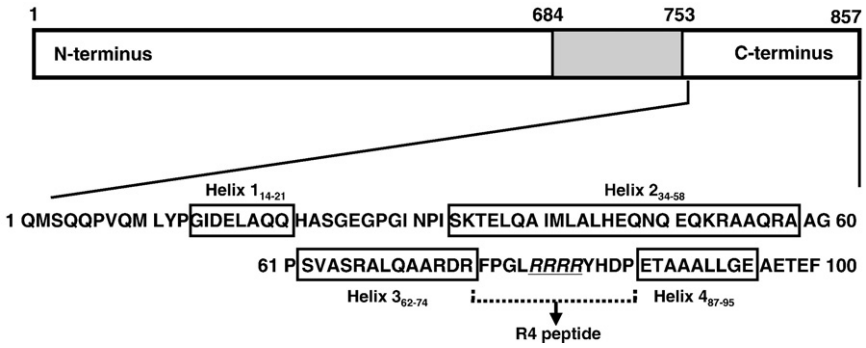

Fig. 1. Schematic representations of EBV gp110 and the C-terminal domain. The coding region for EBV gp110 is represented as an open box with the gray area indicating the putative membrane-spanning domain. The numbers indicate the numbers of gp110 amino acid. The C-terminal domain investigated in this study is depicted with the predicted secondary structural regions. The open boxes in the C-terminal domain represent the putative helices. The secondary structure estimation was carried out using PSIPRED 2.0 (McGuffin et al., 2000). The underlined italic sequence, RRRR represents the nuclear localization signal (NLS) and the arrow indicates the synthesized peptide sequence (R4 peptide) used in the present investigation.

localization signal (NLS) is caused by the altered structure, the conformational difference between the native gp110 CTD and the mutant gp110 CTD containing the mutated NLS was examined.

Results

Folding intermediate of gp110 CTD in buffer conditions

Both the wild-type and mutant gp110 CTD were cleanly purified, as described in Materials and methods. Almost the same procedure was applied to the purification of both proteins. The final yields of the wild-type and mutant proteins were approximately 10 mg and 12 mg per liter of *E. coli* culture, respectively. The SDS-PAGE showed that the purified protein appeared homogeneous (Fig. 2).

Gp110 CTD was not so highly ordered in a buffer condition (Park et al., 2002), even though the presence of two negative extremes at 222 and 205 nm and the positive maximum below 200 nm pointed that the protein adopts a partially helical conformation (Fig. 3). This gp110 CTD showed very little structural change in the buffer solution when pH was changed from 4 to 9 (Fig. 4A). Apparent intensity at 205 nm and 222 nm appeared to be slightly less at pH 8 than at the others, but the ratios of 205/222 nm were almost equal over the pH range investigated. This result suggests that gp110 CTD at various pHs has the same conformational characteristics. However, the Tm curves clearly showed that the tertiary structure of gp110 CTD is not compact (Fig. 4B); as the temperature increasing, the Tm curve gradually increased and reached at plateau about 60 °C. The gradual increase of Tm curve is the general characteristic of unordered or loosely folded proteins. In contrast, various folded proteins show a sigmoid pattern of Tm curves. Thus, this result reveals that the conformation of gp110 CTD in the buffer solution is not highly ordered, even though the protein possesses the structural stability somehow. The effect of ionic strength on the structural stability was also evaluated. The melting temperature of gp110 CTD was not significantly affected by salt concentration, though the slight intensification of CD signal at 222 nm occurred with increasing salt concentration (Fig. 4C). This slight intensification might be caused by the enhanced intramolecular or intermolecular hydrophobic interactions which stabilize the structure of gp110 CTD.

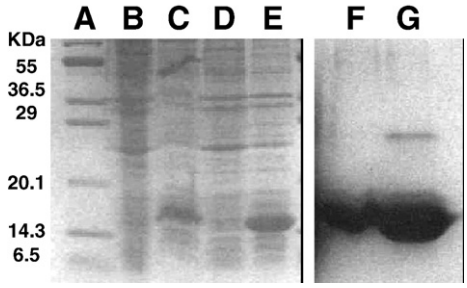

Fig. 2. SDS-PAGE of the recombinant gp110 CTD. Lanes: (A) Molecular markers; (B) The whole-cell lysate of the wild-type gp110 CTD before induction; (C) The whole-cell lysate of the wild-type gp110 CTD after induction; (D) The whole-cell lysate of the mutant gp110 CTD (RT2R) before induction; (E) The whole-cell lysate of the wild-type gp110 CTD after induction; (F) the wild-type gp110 CTD after purification; (G) the mutant gp110 CTD (RT2R) after purification.

Binding to membrane mimics

To identify the binding to membrane mimics, the mobility change of gp110 CTD in micelles and lipid vesicle on a gel column was monitored at 280 nm. As a model membrane, DPC, SDS micelles, and liposome vesicles were used. In the buffer condition, gp110 CTD was eluted as a single peak at 11.83 min (Fig. 5A), which is corresponding to the trimeric molecular weight (approximately 36,000 Da) of gp110 CTD (Table 1). When mixed with micelles and lipid vesicle, the protein was eluted near at void volume (Figs. 5B–E), revealing the protein was complexed with the membrane mimics. Each fraction was analyzed by SDS-PAGE and the presence of gp110 CTD in eluate was confirmed (data not shown). Presumably, DPC and SDS form multi-sized micelles and the population of large micelles is sparse, since the fraction volume of the gp110 CTD-large micelle complex was relatively low. In the case of the multilamella lipid vesicle whose diameter was approximately 150 nm, gp110 CTD binding was clearly detected; the retention time of a bounded complex was shifted from 6.81 min to 5.32 min (Fig. 5E). The fraction at 10.55 min seems to be a complex of gp110 CTD and the relative small vesicles. Because the liposomes contribute to light scattering, the peak volume detected at 280 nm does not exactly indicate the amount of protein associated with the liposomes. Indirectly, the ratios of gp110 CTD associated with large micelles and liposome vesicles were deduced by calculating the peak volume of the remained protein after binding. Table 2 shows that the amount of gp110 CTD bound to DPC or SDS micelles was less than that of the liposome bound form. However, these data do not imply that micelles have lower affinity to gp110 CTD, compared with the result of liposome, since the detectable large micelles on the gel column may not be densely populated in the experimental condition.

Structural transition in membrane-like environment

The structural change in membrane environment was investigated using SDS, DPC micelles, and liposome vesicles (Losonczi et al., 2000; Matthey et al., 1999; Henry and Sykes, 1992; Kochendoerfer et al., 1999; Ruan et al., 1998), which were selected to investigate the

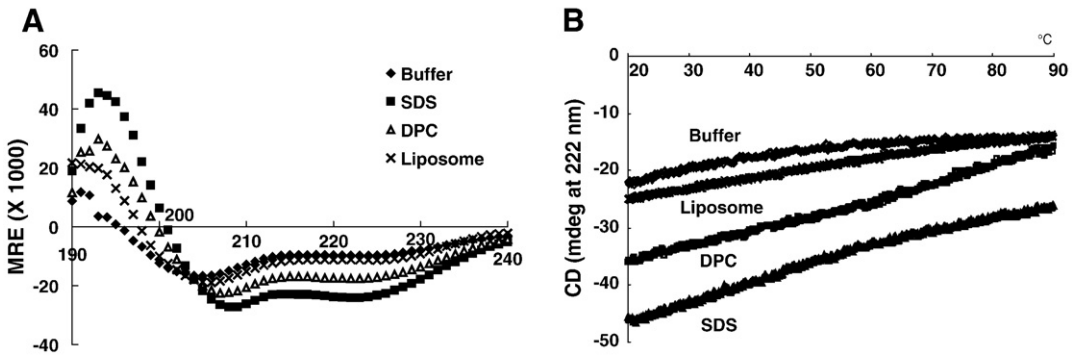

Fig. 3. Induced helicity in membrane mimics. (A) Fifteen μM of gp110 CTD was dissolved in 50 mM DPC, 10 mM SDS micelles, and 10 mM liposome solutions, with 5 mM sodium phosphate. The final pH of each solution was adjusted to 7.4. The spectra were expressed as mean residual molar ellipticity ([θ], deg cm^2/dmol) from 190 to 240 nm by dividing the measured molar ellipticity by the number of residues of gp110 CTD. (B) Tm curves in membrane mimics.

possible influence of the net charge of membrane mimics. The CD spectra of gp110 CTD in membrane mimics exhibited evidence of significant α-helical structure as indicated by the strong positive band at about 190 nm and negative bands near 208 and 222 nm (Fig. 3A). Increasing concentration of micelles and liposome substantially affected the CD curves (data not shown). The presence of isodichroic point at 205 nm indicates a transition from a folding intermediate to a helical structure. Gp110 CTD in the liposome and DPC micelle solution appeared to be slightly less helical than gp110 CTD in the SDS micelle solution (Fig. 3A). The thermal stability of gp110 CTD in membrane mimics was similar to that in the buffer solution: The Tm curves gradually increased regardless of sources of membrane mimics (Fig. 3B). This result indicates the lack of a stable tertiary structure in the membrane-bound state.

The structural transition of gp110 CTD was also observed in the HSQC spectra (Fig. 6). The spectra were acquired at 30 °C in 50 mM sodium phosphate buffer (pH 6.0). In the buffer solution, the distribution of cross-peaks was poor and the amide peaks were largely amassed. The two-dimensional NOESY and TOCSY data were very poor and showed only a few broad and strong cross-peaks (data not shown). However, the NH resonances were dramatically changed in micelle conditions as shown in Figs. 6B, C. Both the DPC and SDS micelles affected the dispersion of NH cross-peaks. Compared to DPC sample, the peak aggregation in the center region was more weakened in SDS sample. In addition, the resolution of peaks highly increased when the NMR sample was deuterated (Fig. 6D). Gp110 CTD has seven Gly residues that were not completely detectable in the buffer and the micelles. However, by deuteration and applying SDS micelles, all Gly residues can be detected in the HSQC spectrum (Fig. 6D). Actually, about 104 peaks can be peaked except side-chain peaks of Gln an Asn, revealing almost all residues were visible in this spectrum.

Comparison of structures between wild-type and mutant gp110 CTD

To verify the structural difference between the wild-type gp110 CTD (R4) and the mutant gp110 CTD of which NLS signal, RRRR was mutated to RTTR (RT2R), the CD experiments were performed in various solution conditions for RT2R. Similar to R4, RT2R showed a well ordered secondary structure in micelle solution (Fig. 7). The partially ordered structure in the buffer solution and the pattern of secondary structural change in the micelles solution indicate the structural characteristic was unaffected by mutation of NLS. However, there were subtle differences between R4 and RT2R. Compared to the R4, the intensification of the CD signals of RT2R was observed. The helicity of the two proteins in various solutions were estimated using the CD signal at 222 nm (Table 3). The helical conformation of RT2R in micelles apparently looks more stabilized than that of R4. However, the 208/222 nm ratio of RT2R in the buffer solution notably increased from 1.54 to 1.64 (Fig. 7).

The structures of two peptides, FPGLRRRRYHDP (R4 peptide) and FPGLRTTRYHDP (RT2R peptide) were determined in SDS micelles for analyzing the effect of amino acids substitution on the configuration of NLS. It was predicted that these peptides correspond to a loop region linking the helix 3 and helix 4 (Fig. 1). These peptides do not seem to adopt any regular structures in both buffer and micelle solutions, based on the CD data (data not shown). This result indicated that the conformations of two peptides were not significantly dependant on the solutions used. The NMR experiments were carried

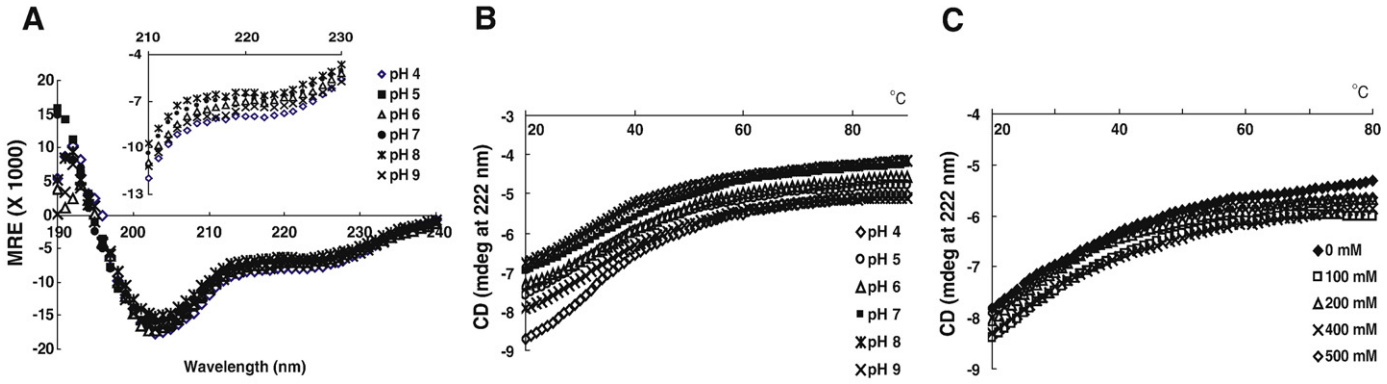

Fig. 4. Effects of pH and salt concentration on the structural and thermal stability. As the temperature increasing, the Tm curve gradually increases and reaches at plateau about 60 °C, which was not changed in various conditions. The experiment on pH effect was conducted with 5 μM of gp110 CTD that was dissolved in 5 mM sodium phosphate buffer with 100 mM NaCl. (A) The pH dependence of the secondary structure. The inset is the expansion of the CD curves from 210 nm to 230 nm. (B) Tm curves at various pHs. (C) Tm curves with increasing NaCl concentration.

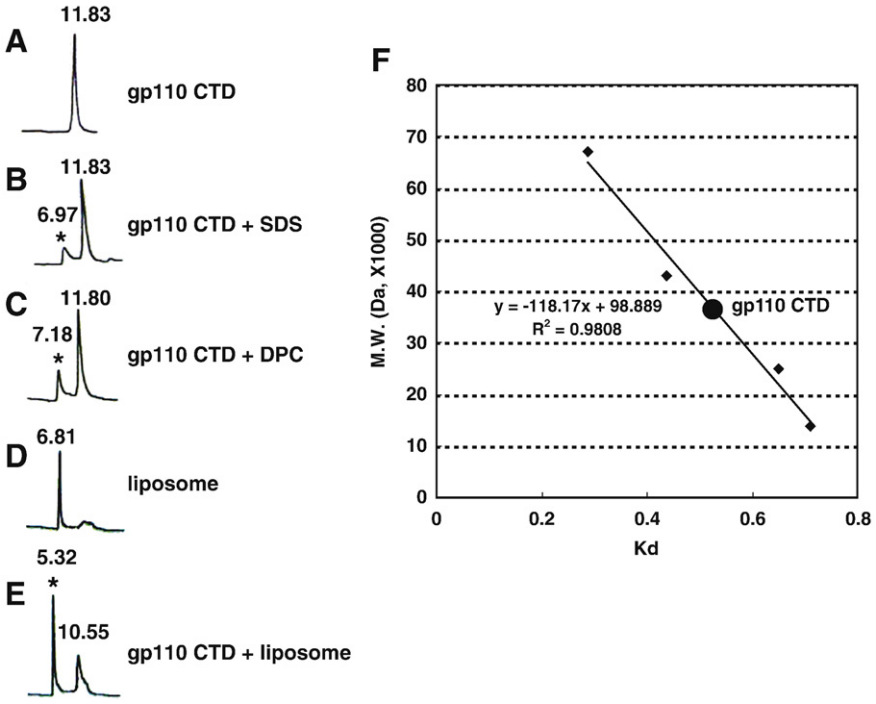

Fig. 5. Elution profiles of size-exclusion chromatography in micelle and lipid solutions. All the injected concentration of gp110 CTD in every mixtures were equally 0.5 mM. (A) gp110 CTD; (B) SDS+gp110 CTD; (C) DPC+gp110 CTD; (D) liposome (PC:PG=3:1) only; (E) liposome+gp110 CTD. Asterisks are the peak fractions containing the mixture of micelle and protein. The number on the each peak is the elution time (minutes at flow rate 1 ml/min). (F) Standard curve obtained in the same buffer without micelles was depicted, and calculated molecular weights were represented in Table 1.

out at 40 °C to overcome the cross-peak overlaps in the ^{1}H dimension. All proton chemical shifts of the R4 and RT2R peptides were unambiguously assigned. The structures of two peptides in SDS micelles were calculated by using distance restraints from NOESY experiments. For the R4 peptide, 180 distance constraints were used in the structure calculations. For the RT2R peptide, a total of 160 distance constraints were used. A set of 100 structures of each peptide was calculated, and the 10 structures with the lowest energy are presented in Fig. 8. These structures had relatively low energies, and there were no NOE violations of >0.5 Å from the distance constraints used in the calculations. Structural statistics for the ensemble of 10 structures of the R4 and RT2R peptides are shown in Table 4. The two peptides adopted similar loops, which did not exhibit a typical turn conformations. The backbone dihedral angles of the NLS (Φ/Ψ angles of 4 residues in the NLS) were −96/−22.5, 65/69.7, 54.8/59.8, and −111.1/−74, while those of the mutant were −105.5/−34.5, 48.7/56.7, −154.6/−32, and 87.4/38.4. When the two models were overlaid around the NLS, they were well superimposed except the N- and C-termini (Fig. 8C). There were little differences in the backbone conformations of the NLSs. The distinct differences were found in the orientation of side-chains. The charged side-chains of four Arg residues in the wild-type peptide are projected to the surface of molecule. The side-chains of two Arg and two Thr residues of the mutant also point towards the surface of molecule. The solvent accessible surfaces of four Arg residues in the R4 peptide were 53.1, 48.1, 60.5, and 53.9%, respectively. Those of two Arg and two Thr residues in the RT2R peptide 59.3, 60.1, 58.9, and 59.3%, respectively, indicating the mutant NLS is slightly more solvent-exposed. However, the side-chains of Arg 5 and Arg 8 in two peptides showed the difference of orientation (Fig. 8D). The charged NH groups of residues, Arg 6, 7, 8 in the wild-type peptide, point the same direction, while those of Arg 5 point toward N-terminus. The side-chains of Arg 5 and Arg 8 in the mutant point toward opposite direction, compared with those of the wild-type. The short side-chains of two Thr residues in the mutant peptide may affect the different orientations of side-chains, since no NOEs from the side-chains of two Thr residues and no steric hindrance exist. As a result, the surface charges of two peptides are differently distributed; the positively charged residues of the R4 peptide are more concentrated on one region, compared to the RT2R peptide (Figs. 8E, F).

Table 1
Elution profile of molecular standards and gp110 CTD

Samples		M.W. (Da)	Retention time (V_r, min)	Kd[a] (Distribution coefficient)
1Molecular standards	Blue dextran	1,000,000	6.69	Void vol. (V_0)
	Albumin	67,000	9.51	0.29
	Ovalbumin	43,000	10.98	0.44
	Chymotrypsin	25,000	13.05	0.65
	Ribonuclease	13,700	13.65	0.71
	Tyrosine	204	16.47	Column vol. (V_t)
Gp110 CTD		36,783[b]	11.83	0.53

[a] $Kd=(V_r-V_0)/(V_t-V_0)$.
[b] Estimated molecular weight was calculated from the standard curve depicted in Fig. 4F.

Discussion

The current study suggests that the C-terminal domain is not so highly ordered on its own and forms more ordered structure upon interaction with membranes. The structure of gp110 CTD in the buffer solution was partially folded and was not affected by pH or salt concentrations. In addition, the gel column profile showed this protein in the buffer solutions exists as a trimer, revealing that the trimerization region of gp110 exists in the C-terminal domain. It is

Table 2
The amounts of gp110 CTD associated with large micelles and liposome vesicles

Complex media	DPC	SDS	Liposome
Fraction %	20[a]	14[a]	40[a]

[a] The fraction % was calculated by the peak volume of a complex divided by the peak volume of the control gp110 CTD (Fig. 4A).

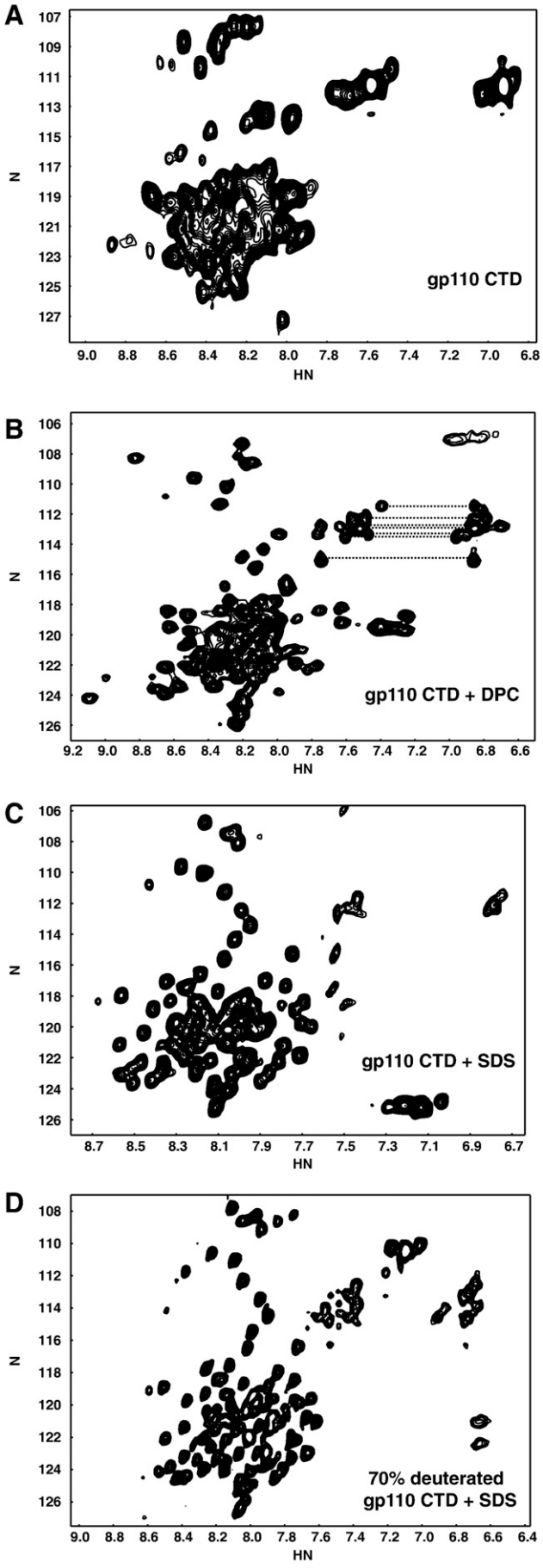

very interesting that gp110 CTD forms a trimeric complex like the ectodomain of HSV gB (Heldwein et al., 2006; Backovic et al., 2007). The trimerization of gp110 CTD affected the spin-relaxation times, since the deuteration of the NMR sample enhanced the line broadening in the HSQC spectrum (Fig. 6D). The alteration of the trimer state seems not to be derived by pH and ionic strength, considering that the thermal denaturation profiles were almost identical in various conditions (Fig. 4). Therefore, the trimeric structure of gp110 CTD in the buffer solutions appears to be a folding intermediate that lacks compactness. Even in membrane mimics, a stable tertiary structure of gp110 CTD does not seem to be formed, while the helical property dramatically increased.

This conformational characteristic is very similar with that of molten-globules; the molten globules generally retain their secondary structure, while they lack some or all tertiary structure (Ptitsyn, 1995; Dobson, 1994). The molten-globular state is related to membrane binding capacity in membrane proteins. In some cases, the native molten-globular structures facilitate binding to lipid bilayer membranes at neutral pH (Park et al., 2002; Song et al., 2001; Lohner and Esser, 1991). Occasionally, membrane binding induces the molten-globular structure (Muga et al., 1991; van der Goot et al., 1991; Banuelos and Muga, 1995): the acidic molten-globular state could be an intermediate formed during the insertion of colicin A into membranes (van der Goot et al., 1991). The α-lactalbulmin associates with the negatively charged membranes accompanying a molten-globule like conformational change (Banuelos and Muga, 1995).

In case of gp110 CTD, membrane mimics induce the highly helical conformation: the increased helicity of the membrane-associated conformers indicates that the relatively unstructured segments of the protein adopt a helical conformation upon binding to membrane (Fig. 3). The helical content of the protein seems to be affected by the size of membrane mimics. Compared with DPC and SDS micelles, the large liposome induced relatively low helicity (Table 3). However, the membrane binding capacity of gp110 CTD was well maintained in the liposome vesicle, based on the gel column profile. The most helical structure was derived in the SDS micelles, which reveals that the negative charge of micelles as well as the size of membrane mimics significantly affects the helical content of gp110 CTD. In addition, this structural change in membrane environment can be found in the HSQC spectrum (Fig. 6), since the chemical shift changes directly reflect the structural change. Consistent with CD results, the spectrum showed large signal changes in micelle solutions, implying that the conformational change is significant in membrane environment.

It is not clear whether the helical structure induced by membrane mimics correlates with the membrane insertion and/or protein translocation across membranes. However, several studies support the increased helicity is required in protein insertion and/or translocation to membranes (Song et al., 2001; Muga et al., 1991; Banuelos and Muga, 1995). Apocytochrome *c* undergoes a transition from an essentially unordered conformation in solution to an alpha-helical structure in a model membrane (Muga et al., 1991). The interaction of the steroidogenic acute regulatory protein (StAR) with membranes is facilitated by the induced helicity (Song et al., 2001). A similar folding behavior was described for interaction of α-lactoalbumin with negatively charged membranes (Banuelos and Muga, 1995). Thus, the helical nature in membrane mimics may reflect an association mechanism of gp110 with membranes.

The nuclear localization of gp110 is mediated by the NLS (RRRR) in the C-terminal domain. The former study revealed that these four

Fig. 6. Two-dimensional $^{1}H/^{15}N$ HSQC spectra of gp110 CTD with or without micelles. The protein concentration was 1.2 mM. The sample was dissolved in 50 mM sodium phosphate buffer, 150 mM NaCl (pH 6.0). The spectra were acquired at 303 K. The dotted lines represent the side-chain amide peaks. The side-chain amides of glutamines and asparagines exhibit more amassed cross-peaks in the presence of DPC micelles. (A) Without DPC micelles. (B) With DPC micelles (100 mM deuterated DPC). (C) With SDS micelles (200 mM deuterated SDS). (D) 70% duterated gp110 in SDS micelles.

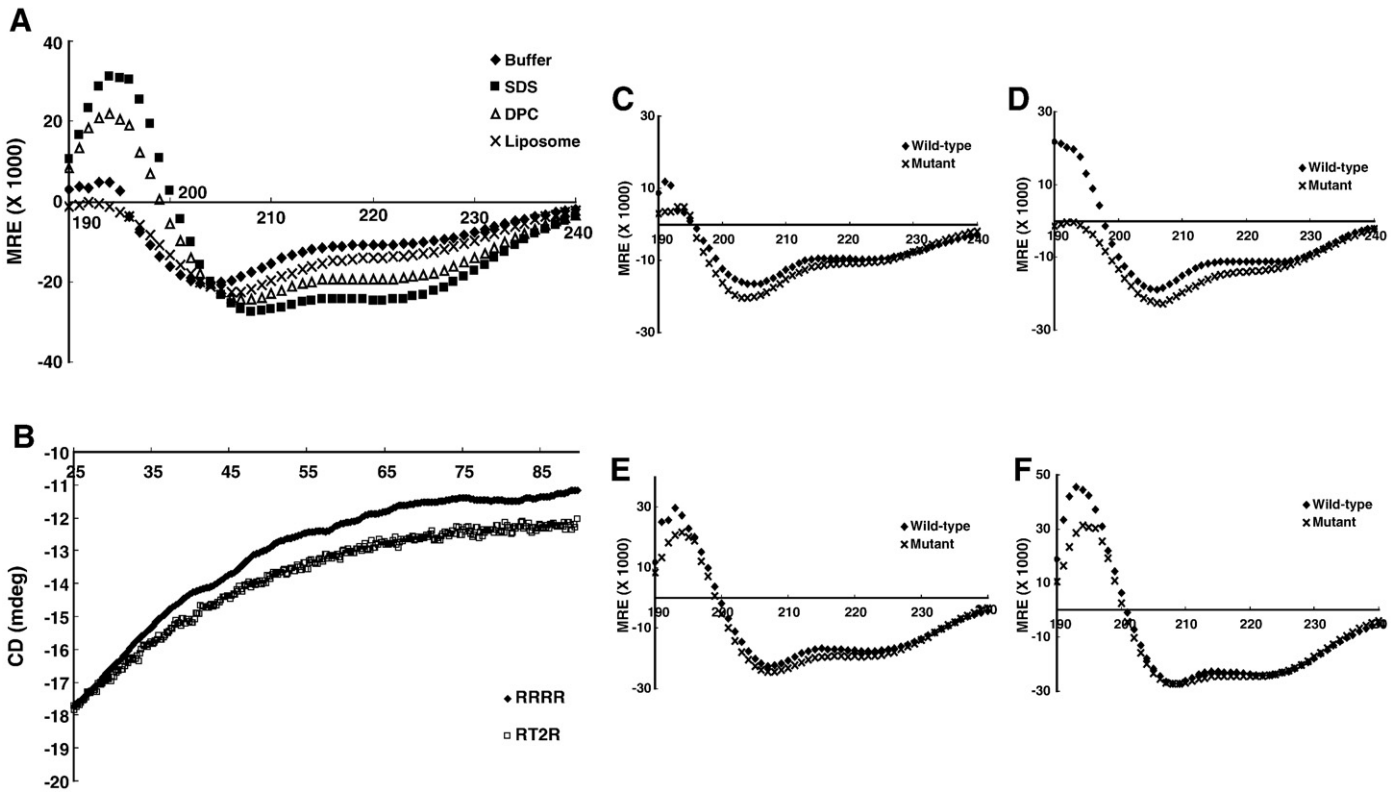

Fig. 7. Comparison of CD spectra between wild-type and mutant gp110 CTDs. The spectra are expressed as mean residual molar ellipticity ([θ], deg cm^2/dmol) from 190 to 240 nm by dividing the measured molar ellipticity by the number of residues in gp110 CTD. The Tm curve is expressed as ellipticity (mdeg) at 222 nm. (A) superimposed CD spectra of mutant; (B) Tm curves of two forms; CD spectra of wild-type and mutant forms were compared in the buffer solution (C), in liposome (D), in DPC micelles (E), and in SDS micelles (F).

arginine residues are the only important sequences for the ER/nuclear localization (Lee and Longnecker, 1997; Lee, 1999). The mutation of the NLS resulted in the change of intracellular localization and the alteration of glycosylation pattern; the mutant gp110 containing either KKKK, REER, or RTTR failed to localize the ER/nuclear membrane while the arginine to lysine substitution at the second position of NLS (RKRR) did not disturb the ER/nuclear localization pattern of gp110 (Lee, 1999). The failure of the ER/nuclear localization by the C-terminal mutation results in the increased expression on the plasma membrane. Interestingly, more recent studies suggest that gp110 plays a role in EBV entry to a target cell by endocytosis and/or direct cell fusion and the region containing the NLS negatively regulates the ability of gp110 to induce membrane fusion (McShane and Longnecker, 2004; Haan et al., 2001). These results indicate that not only the net charge but also the conformation of the four arginines are important for the subcellular localization of gp110 and EBV membrane fusion.

To elucidate that the disturbed localization is related to the conformational difference between the wild-type and the mutant gp110 CTD, the structural feature of the mutant gp110 CTD containing RTTR (RT2R in this paper) was investigated. The structural characteristic of the mutant gp110 CTD was very similar to that of the wild-type; the formation of the folding intermediate in the buffer solution as well as the structural change in the membrane mimics, were equally identified. However, the helical content of RT2R was slightly different in the buffer condition, compared with R4. On the contrary, the overall conformation in the membrane mimics was very similar to that of the wild-type protein, since the ratio of 208/222 nm of two proteins in the CD data did not show a significant difference. Thus, the overall structural difference between the wild-type and the mutant forms was found only in the buffer condition while the difference in membrane environment may be restricted to the local region around the NLS motif. Consistent with this observation, the structures of two peptides, R4 and RT2R, were similar each other except the side-chain orientation and both ends of peptides. This result reveals that the helicity induced in membrane environment is not directly related to trafficking to ER/nuclear membrane.

Table 3
Comparison of ratio of 208/222 nm and estimated α-helicity between wild-type and mutant gp110

Sample	Buffer	DPC	SDS	Liposome
Wild-type	1.54 (23%)[a]	1.27 (51%)	1.13 (74%)	1.56 (31%)
Mutant	1.64 (27%)	1.27 (56%)	1.12 (76%)	1.58 (38%)

[a] The estimated values of α-helicity that were calculated with CD signals at 222 nm, are indicated in parentheses.

The overall structural similarity between RT2R and R4 in membrane mimics is consistent with the fusion activity of gp110 (McShane and Longnecker, 2004; Haan et al., 2001): in a virus-free cell fusion assay, the mutant gp110 CTD exhibited the ability to mediate membrane fusion similar to that of the wild-type protein (McShane and Longnecker, 2004). R4 and RT2R peptides, showing similar backbone structures except side-chain orientation, also support that the mutation at the NLS had no effect on membrane fusion.

As described earlier, gp110 localizes both the inner and outer nuclear membrane. To reach the inner nuclear membrane, gp110 may diffuse laterally along the pore membrane. Indeed, some viral membrane proteins freely diffuse across the nuclear pore membrane (Torrisi et al., 1987; Holmer and Worman, 2001; Lusk et al., 2007). However, some studies suggested that transport of integral membrane proteins to the inner membrane requires a signal-

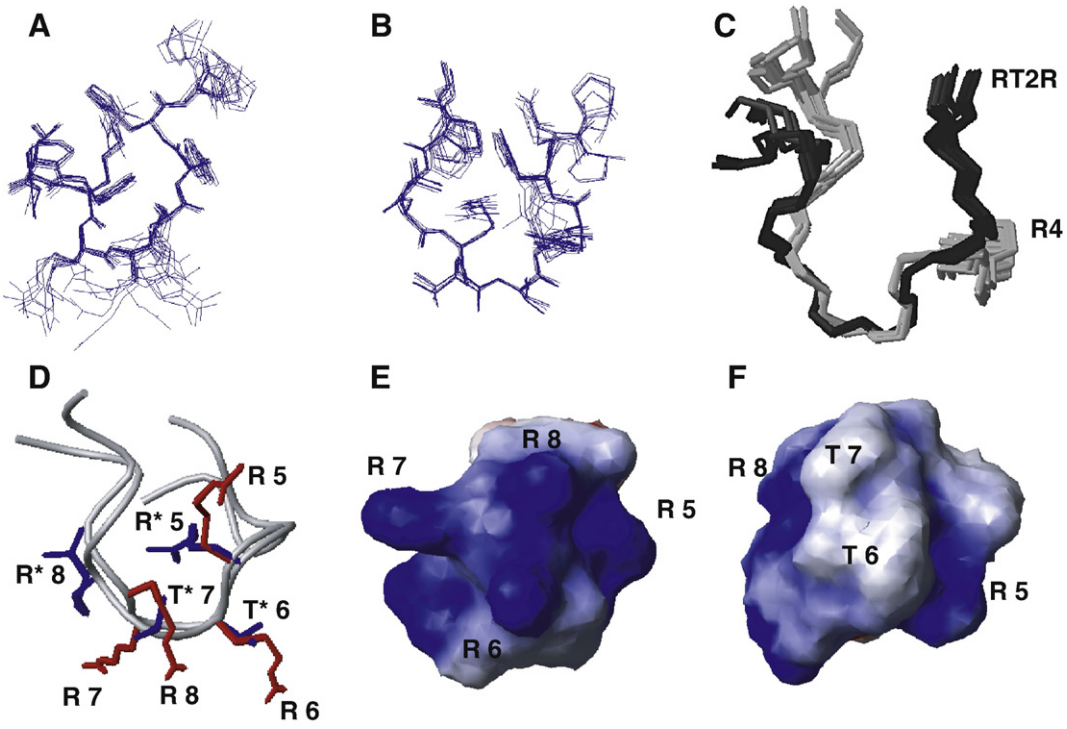

Fig. 8. Structural comparison between the R4 and RT2R peptides. Ensembles of 10 torsion angle dynamics conformers of the R4 peptide (A) and the RT2R peptide (B) are depicted. The backbones from the ensemble structures of the R4 (gray) and RT2R (black) peptides are overlaid (C). The orientations of the four arginines (red) in the NLS motif of the R4 peptide are compared with those (blue) of the RT2R peptide (D). The asterisks represent the residues from the RT2R peptide. The electrostatic potential surfaces of the R4 (E) and the RT2R (F) peptides are compared. The positively charged residues are represented in blue. The program MolMol was used for this presentation. (For interpretation of the references to colour in this figure legend, the reader is referred to the web version of this article.)

mediated transport pathway (Lusk et al., 2007; King et al., 2006; Braunagel et al., 2007; Saksena et al., 2006).

For the most cellular proteins, NLS-dependent translocation across NPC is mediated by the binding of an NLS on cargo proteins to importin-α in the cytoplasm (Fontes et al., 2000, 2003; Rowland and Yoo, 2003). The structural studies of monopartite and bipartite NLS recognition by importin-α showed that the two basic clusters of bipartite NLSs bind to two separate binding sites on importin-α. In addition, monopartite NLS can bind to both sites but preferentially use one binding site, referred as the major site (Fontes et al., 2000, 2003). Very interestingly, the R4 peptide shares the structural similarity with the monopartite NLS of the simian virus 40 (SV40) large T-antigen, $_{126}$PKKKRKV$_{132}$ (Fig. 9A). The monopartite SV40 NLS bound to importin-α adopts an extended conformation and the basic side-chains of the NLS interact with the negatively charged residues of importin-α (Fontes et al., 2000, 2003). The structure of the R4 peptide adopts a loop, rather than an extended conformation. However, we found that the side-chain orientations of NLS were very similar to that of SV40 large T-antigen. Fig. 9A shows that the side-chains of the repeated arginine or lysine point the same directions, except the Arg 5 of the NLS in gp110 CTD.

In addition to this observation, a recent study demonstrated that the yeast inner nuclear membrane proteins with the classical NLS sequence are also transported by the karyopherins complex (importin-α and -β complex) via the nuclear pore complex (NPC) (King et al., 2006). Therefore, these results may provide that the importin-mediated transport is one of possible routes for gp110's nuclear localization, especially for the inner membrane localization (Fig. 9B).

Table 4
Structural statistics for the ensemble of 10 structures of R4 and RT2R peptides

Statistics for structure calculations	R4	RT2R
R.m.s.d. from idealized covalent geometry		
Bonds (Å)	0.0012±0.00083	0.0018±0.00016
Bond angles (°)	0.4407±0.0057	0.4842±0.0093
Improper torsions (°)	0.0870±0.0112	0.1222±0.016
R.m.s.d. from experimental restraints		
Distances (Å)	0.037±0.0014	0.0047±0.0007
Final energies (kcal mol^{-1})		
E_{total}	15.91±0.73	22.61±1.87
E_{bond}	0.31±0.06	0.65±0.13
E_{angles}	12.01±0.31	13.29±0.51
E_{vdw}	3.22±0.28	8.09±1.14
E_{imp}	0.16±0.04	0.27±0.07
E_{NOE}	0.21±0.15	0.32±0.09
Average R.m.s.d. to the mean structure for all heavy atoms/the backbone (Å)	1.18/0.19	0.75/0.27

Materials and methods

Materials

Restriction endonucleases were purchased from New England Biolabs Inc. (Beverly, MA, USA), and Promega (Madison, WI, USA). Cloned *Pfu* DNA polymerase was obtained from Stratagene (La Jolla, CA, USA). Dodecyl phosphocholine (DPC) was purchased from Avanti Polar Lipids Inc. (Alabaster, AL, USA). Sodium dodecyl sulfate (SDS) was obtained from Sigma (St. Louis, MO, USA). All materials were of reagent or biotechnological grade.

Plasmids construction and expression

The plasmid carrying the sequence coding for gp110 CTD (including amino acid 758 to 857 of EBV gp110) was constructed. The plasmid pJ4-m encoding the C-terminal gp110 (Park et al., 2002) was used as a template to prepare gp110 CTD constructs. The plasmid was generated by inserting the PCR fragment into the NdeI–XhoI digested pET-21a and designated as pGP110C. The resulting protein product has a His_6 C-terminal tag. For mutation analysis, the RRRR

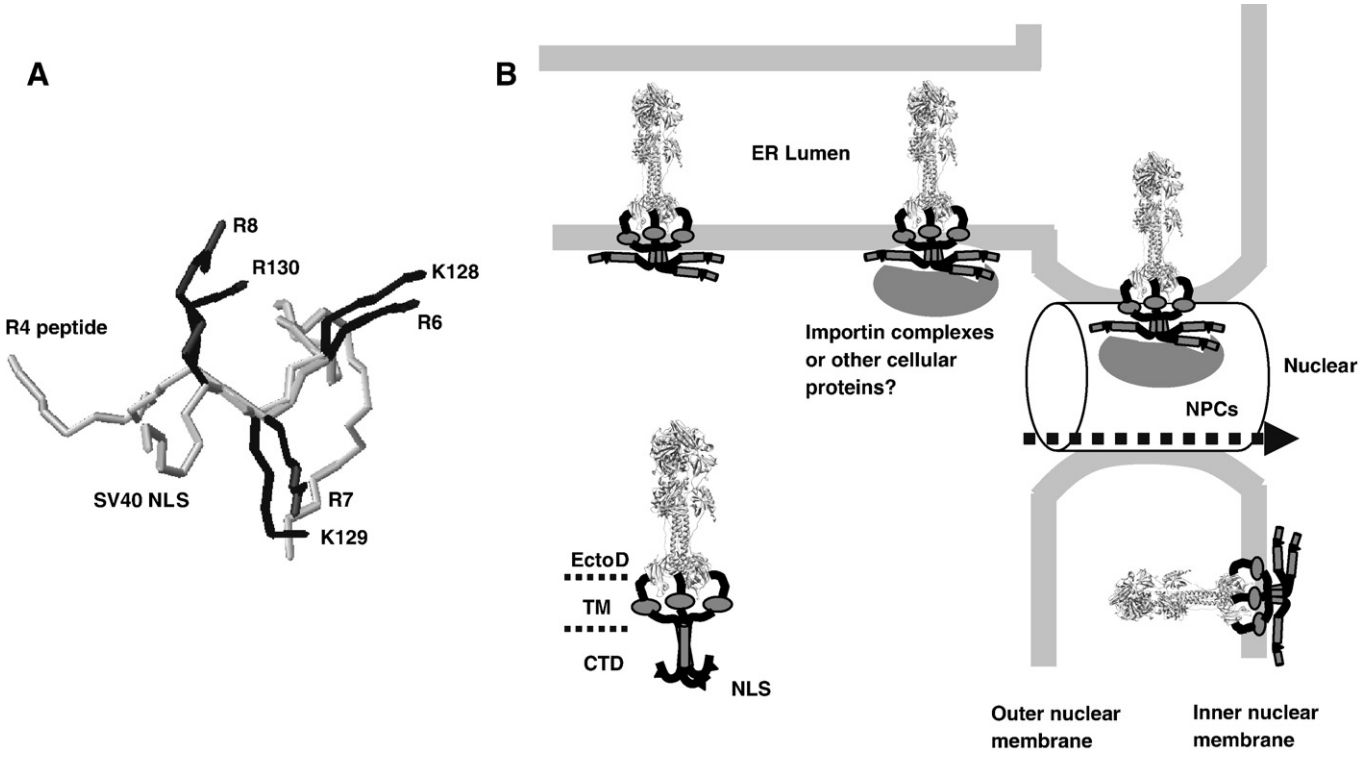

Fig. 9. Schematic representation for the nuclear localization of gp110. The neon diagrams of the R4 peptide and the importin-α-bound monopartite NLS of the simian virus 40 (SV40) large T-antigen, $_{126}$PKKKRKV$_{132}$ are superimposed (A). The model of the R4 peptide is the energy-minimized average structure. The crystal structure of the monopartite NLS of SV40 (PDB ID:1EJL) were obtained from the Protein Data Bank (PDB). The orientation of the three arginines in the NLS motif of gp110 CTD is compared with those of the monopartite NLS of SV40. The subcellular localization of gp110 is schematically depicted (B). The crystal structure of the ectodomain of glycoprotein B from Herpes Simplex Virus 1 was obtained form PDB (2GUM). EctoD: ectodomain of gB; TM: transmembrane domain of gp110; CTD: c-terminal domain of gp110; NPC: nuclear pore complex.

sequence was exchanged to RTTR. The consecutive AGA codons were replaced with the major threonine ACC codons by site-directed mutagenesis. PCR amplification was performed with *pfu* DNA polymerase using two overlapping primers, 5′-GTTTTCCAGGCCTACG-CACCACCCGCTATCACGATG-3′ (sense) and 5′-GATCGTGATAGCGGG-TGGTGCGTAGGCCTGGAAAAC-3′ (antisense) containing the threonine codons (underlined). The constructed plasmids were confirmed by restriction analysis and DNA sequencing. The wild-type gp110 CTD is referred as R4 and the mutant as RT2R hereafter.

The constructs were transformed into *E. coli* BL21 (DE3) and cultured in the LB broth or in the M9 (^{15}N) media. After incubation at 37 °C for 7 h, protein expression was induced by adding isopropyl β-D-1-thiogalactopyranoside (IPTG) to a final concentration of 1 mM. After 4 h postinduction at 37 °C, cells were harvested by centrifugation with 8000 rpm at 4 °C for 15 min (Beckman J2-MC).

Purification of R4 and RT2R

The bacterial cell pellets were suspended in 100 ml of the lysis buffer (50 mM Tris–Cl (pH 7.9), 500 mM NaCl, 10% glycerol, and 1 tablet of EDTA-free protease inhibitor cocktail (Roche) containing 0.2 mg/ml lysozyme. The bacterial lysis was performed by sonication (4×30-s pulses) until the lysate became clear. After lysis, the supernatant was applied to a His-tag column (2.5×20 cm). Bound proteins were eluted with a linear 50–800 mM immidazole gradient at the flow rate of 1 ml/min. After pooling the eluted fractions, the protein solution was dialyzed with a buffer (25 mM sodium phosphate (pH 7.5), 50 mM NaCl, and 1 mM PMSF (phenylmethylsulphonyl fluoride). The dialyzed solution was applied to the Q-Sepharose ion-exchange chromatography (Amersham Pharmacia Biotech, Uppsala, Sweden) and eluted with a linear 50–600 mM NaCl gradient in the sodium phosphate buffer. Protein samples were collected at each purification step and analyzed by SDS-PAGE. The same procedure was applied for purification of the mutant gp110 CTD. All purification steps were conducted in a cold room. The purified gp110 CTD was stored in the buffer, 25 mM sodium phosphate (pH 6.0) containing 1 mM PMSF and 300 mM NaCl since the gp110 CTD is relatively stable at high salt concentration.

Preparation of phospholipids liposome

Liposome of PC and PG mixture (3:1 molar ratio) was prepared. Egg yolk L-α-L-phosphatidylcholine (egg PC) and L-α-phosphatidyl-DL-glycerol which was enzymatically converted from egg PC (egg PG) were purchased from Avanti (Alabaster, AL) and each were prepared in a chloroform solution and a chloroform/methanol (2/1) solution. The solvent was evacuated for at least 1 h and evaporated under nitrogen gas flow to remove any remaining trace of the solvent. The dried lipid films on the inner walls of the round bottom flask were hydrated with a buffer solution [10 mM Tris, 150 mM NaCl, 1 mM EDTA (pH 7.0)] and vortex mixed to produce the MLVs (Multi lamellar vesicles). The suspension was freeze–thawed for five cycles and then extruded through polycarbonate filters (a 0.1 μm pore size filters, 10 times). The lipid concentration was determined by Stewart assay (Charles and Stewart, 1980).

Gel-permeation chromatography

DPC, SDS micelles (100 mM and 200 mM, respectively), and Phospholipid liposome (10 mM) were mixed with gp110 CTD (1.2 mM) in 10 mM sodium phosphate buffer (pH 6.5) respectively and each mixture was incubated at 25 °C for 1 h. These mixture (50 μl) were injected onto a Biosep S-3000 (Phenomenex), connected to a Hitachi L 6200 HPLC and pre-equilibrated with the same buffer. The each mixture contained equal amount of gp110 CTD; the final concentration of gp110 CTD in 50 μl injection volume was 0.5 mM. The elution at

1 ml/min was monitored at 280 nm. Each peak was collected and the fractions were analyzed by SDS-PAGE.

Circular dichroism analysis

Circular dichroism (CD) analysis was performed by using Jasco J-715 spectropolarimeter at 20 °C. CD measurements were carried out in a wavelength range between 190 nm and 240 nm. The gp110 CTD purified as described above was dialyzed against 5 mM sodium phosphate buffer (pH 7.4) and concentrated using a Centricon 30 unit (Amicon Inc., Beverly, MA, USA). The resultant spectra were corrected for the buffer signal. To examine the structural change in membrane-mimicking environment, the spectra of gp110 CTD (5–15 μM) were also collected in 5 mM sodium phosphate buffer (pH 7.4) with 50 mM DPC, 10 mM SDS, and 10 mM phospholipids liposome. A baseline of pure micelle solution was recorded and subtracted from each spectrum. Estimation of α-helicity percent was made using a method modified by Wu et al. (1981) and Chen et al. (1974). This method uses ellipticities at either 208 or 222 nm and calculates fractional helicities as follows:

$$f_h = \left(\theta_{222} - \theta^0_{222}\right) / \left(\theta^{100}_{222} - \theta^0_{222}\right)$$

where θ_{222} is the experimentally observed mean residue ellipticity at 222 nm and values for θ^0_{222} and θ^{100}_{222}, corresponding to 0 and 100% helical content at 222 nm, were estimated to be 2000 and 30,000 deg cm^2/dmol, respectively (Wu et al., 1981; Chen et al., 1974).

NMR spectroscopy

All NMR spectra were acquired by using a 500 MHz Bruker DMX spectrometer equipped with a pulsed-field gradient unit and an actively shielded *z*-gradient triple resonance probe (5 mm or 8 mm). [^{15}N]-gp110 CTD in 50 mM sodium phosphate buffer (90% H_2O/10% D_2O, pH 6.0), in 100 mM DPC/50 mM sodium phosphate buffer (90% H_2O/10% D_2O, pH 6.0), and in 200 mM SDS/50 mM sodium phosphate buffer (90% H_2O/10% D_2O, pH 6.0) were prepared at the concentration of 1 mM. The ^{1}H, ^{15}N-HSQC spectrum of each sample was acquired at 303 K.

Two peptides, FPGLRRRRYHDP and FPGLRTTRYHDP were chemically synthesized. The samples for NMR measurements were prepared by dissolving the synthetic peptides to the concentration of 2 mM in 300 mM SDS-d_{25} (Aldrich). There was no significant difference between the CD spectra of each peptide at pH 4.0 and at pH 7 (data not shown), so that the NMR samples were prepared at pH 4.0 to detect amide proton more easily. The homonuclear DQF-COSY, TOCSY, and NOESY spectra of each peptide were acquired at 40 °C. Data matrices contained 4 K×512 points and 64 scans were accumulated. The 2D TOCSY spectrum was acquired with the mixing time of 60 ms and the 2D NOESY spectrum was acquired with the mixing times of 200 ms. Assignment of the spin-systems to individual amino acids was achieved using DQF-COSY and TOCSY spectra. Proton chemical shifts were referenced to the methyl signal of 2, 2-dimethylsilapentane-5-sulfonic acid (DSS) externally. ^{15}N chemical shifts were indirectly referenced to DSS. All NMR spectra were processed using NMRPipe/NMRDraw and analyzed using NMRView.

For structure calculation of two peptides, distance restraints were obtained from the NOESY spectrum. The NOE data from the NOESY spectrum were classified into three classes; strong, medium, and weak, corresponding to upper bound inter-proton distance restraints of 3.0, 4.0, and 5.0 Å, respectively. Lower distance bounds were taken as the sum of the van der Waals radii of 1.8 Å. The 3-dimensional structures were calculated using the simulated annealing and energy minimization protocol in the program, CNS 1.1.

Acknowledgments

This work was supported by the Korea Science and Engineering Foundation(KOSEF) grant funded by the Korea government(MOST) (Innovative Drug Research Center for Metabolic and Inflammatory Disease). This work also supported in part by 2007 BK21 project for Medicine, Dentistry, and Pharmacy. Korea Basic Science Institute (KBSI) and National Center for Inter-university Research Facilities (NCIRF) kindly supported this work with NMR machines.

References

Backovic, M., Leser, G.P., Lamb, R.A., Longnecker, R., Jardetzky, T.S., 2007. Characterization of EBV gB indicates properties of both class I and class II viral fusion proteins. Virology 368, 102–113.

Banuelos, S., Muga, A., 1995. Binding of molten globule-like conformations to lipid bilayers. Structure of native and partially folded alpha-lactalbumin bound to model membranes. J. Biol. Chem. 270, 29910–29915.

Braunagel, S.C., Williamson, S.T., Saksena, S., Zhong, Z., Russell, W.K., Russell, D.H., Summers, M.D., 2007. Trafficking of ODV-E66 is mediated via a sorting motif and other viral proteins: facilitated trafficking to the inner nuclear membrane. Proc. Natl. Acad. Sci. U.S.A. 101, 8372–8377.

Charles, J., Stewart, M., 1980. Colorimetric determination of phospholipids with ammonium ferrothiocyanate. Anal. Biochem. 104, 10–14.

Chen, Y.H., Yang, J.T., Chau, K.H., 1974. Determination of the helix and beta form of proteins in aqueous solution by circular dichroism. Biochemistry 13, 3350–3359.

Dobson, C.M., 1994. Protein folding. Solid evidence for molten globules. Curr. Biol. 4, 636–640.

Fontes, M.R., Teh, T., Jans, D., Brinkworth, R.I., Kobe, B., 2003. Structural basis for the specificity of bipartite nuclear localization sequence binding by importin-alpha. J. Biol. Chem. 278, 27981–27987.

Fontes, M.R., Teh, T., Kobe, B., 2000. Structural basis of recognition of monopartite and bipartite nuclear localization sequences by mammalian importin-alpha. J. Mol. Biol. 297, 1183–1194.

Haan, K.M., Lee, S.K., Longnecker, R., 2001. Different functional domains in the cytoplasmic tail of glycoprotein B are involved in Epstein–Barr virus-induced membrane fusion. Virology 290, 106–114.

Heldwein, E.E., Lou, H., Bender, F.C., Cohen, G.H., Eisenberg, R.J., Harrison, S.C., 2006. Crystal structure of glycoprotein B from herpes simplex virus 1. Science 313, 217–220.

Henry, G.D., Sykes, B.D., 1992. Assignment of amide 1H and 15N NMR resonances in detergent-solubilized M13 coat protein: a model for the coat protein dimer. Biochemistry 31, 5284–5297.

Holmer, L., Worman, H.J., 2001. Inner nuclear membrane proteins: functions and targeting.Cell Mol. Life Sci. 58, 1741–1747.

King, M.C., Lusk, C.P., Blobel, G.K., 2006. Karyopherin-mediated import of integral inner nuclear membrane proteins. Nature 442, 1003–1007.

Kochendoerfer, G.G., Salom, D., Lear, J.D., Wilk-Orescan, R., Kent, S.B.H., DeGrado, W.F., 1999. Total chemical synthesis of the integral membrane protein influenza A virus M2: Role of its C-terminal domain in tetramer assembly. Biochemistry 38, 11905–11913.

Lee, S.K., 1999. Four consecutive arginine residues at positions 836-839 of EBV gp110 determine intracellular localization of gp110. Virology 264, 350–358.

Lee, S.K., Longnecker, R., 1997. The Epstein–Barr virus glycoprotein 110 carboxy-terminal tail domain is essential for lytic virus replication. J. Virol. 71, 4092–4097.

Lee, S.K., Compton, T., Longnecker, R., 1997. Failure to complement infectivity of EBV and HSV-1 glycoprotein B (gB) deletion mutants with gBs from different human herpesvirus subfamilies. Virology 237, 170–181.

Lohner, K., Esser, A.F., 1991. Thermal unfolding and aggregation of human complement protein C9: a differential scanning calorimetry study. Biochemistry 30, 6620–6625.

Losonczi, J.A., Olejniczak, E.T., Betz, S.F., Harlan, J.E., Mack, J., Fesik, S.W., 2000. NMR studies of the anti-apoptotic protein Bcl-x_L in micelles. Biochemistry 39, 11024–11033.

Lusk, C.P., Blobel, G., King, M.C., 2007. Highway to the inner nuclear membrane: rules for the road. Nat. Rev. Mol. Cell Biol. 8, 414–420.

Matthey, U., Kaim, G., Braun, D., Wüthrich, K., Dimroth, P., 1999. NMR studies of subunit c of the ATP synthase from *Propionigenium modestum* in dodecylsulphate micelles. Eur. J. Biochem. 261, 459–467.

McGuffin, L.J., Bryson, K., Jones, D.T., 2000. The PSIPRED protein structure prediction server. Bioinformatics 16, 404–405.

McShane, M.P., Longnecker, R., 2004. Cell-surface expression of a mutated Epstein–Barr virus glycoprotein B allows fusion independent of other viral proteins. Proc. Natl. Acad. Sci. U.S.A. 101, 17474–17479.

Muga, A., Mantsch, H.H., Surewicz, W.K., 1991. Apocytochrome *c* interaction with phospholipid membranes studied by Fourier-transform infrared spectroscopy. Biochemistry 30, 2629–2635.

Park, S.J., Lee, S.K., Lee, B.J., 2002. Effect of tandem rare codon substitution and vector–host combinations on the expression of the EBV gp110 C-terminal domain in *Escherichia coli*. Protein Expr. Purif. 24, 470–480.

Ptitsyn, O.B., 1995. Structures of folding intermediates. Curr. Opin. Struct. Biol. 5, 74–78.

Rowland, R.R., Yoo, D., 2003. Nucleolar-cytoplasmic shuttling of PRRSV nucleocapsid protein: a simple case of molecular mimicry or the complex regulation by nuclear import, nucleolar localization and nuclear export signal sequences. Virus Res. 95, 23–33.

Ruan, K.-H., Li, D., Ji, J., Lin, Y.-Z., Gao, X., 1998. Structural characterization and topology of the second potential membrane anchor region in the thromboxane A2 synthase amino-terminal domain. Biochemistry 37, 822–830.

Saksena, S., Summers, M.D., Burks, J.K., Johnson, A.E., Braunagel, S.C., 2006. Importin-alpha-16 is a translocon-associated protein involved in sorting membrane proteins to the nuclear envelope. Nat. Struct. Mol. Biol. 13, 500–508.

Song, M., Kim, H., 1997. Stability and solvent accessibility of SecA protein of *Escherichia coli*. J. Biochem. (Tokyo). 122, 1010–1018.

Song, M., Shao, H., Mujeeb, A., James, T.L., Miller, W.L., 2001. Molten-globule structure and membrane binding of the N-terminal protease-resistant domain (63–193) of the steroidogenic acute regulatory protein (StAR). Biochem. J. 356, 151–158.

Torrisi, M.R., Lotti, L.V., Pavan, A., Migliaccio, G., Bonatti, S., 1987. Free diffusion to and from the inner nuclear membrane of newly synthesized plasma membrane glycoproteins. J. Cell Biol. 104, 33–37.

van der Goot, F.G., Gonzalez-Manas, J.M., Lakey, J.H., Pattus, F., 1991. A 'molten-globule' membrane-insertion intermediate of the pore-forming domain of colicin A. Nature 354, 408–410.

Wu, C.S.C., Ikeda, K., Yang, J.T., 1981. Ordered conformation of polypeptides and proteins in acidic dodecyl sulfate solution. Biochemistry 20, 566–570.